Second Virial Coefficient of Oligo- and Poly(methyl methacrylate)s. Effects of Chain Stiffness and Chain Ends

Fumiaki Abe, Yoshiyuki Einaga, and Hiromi Yamakawa*

Department of Polymer Chemistry, Kyoto University, Kyoto 606-01, Japan

Received December 29, 1993; Revised Manuscript Received March 21, 1994®

ABSTRACT: The second virial coefficient A_2 was determined for atactic poly(methyl methacrylate) (a-PMMA) over a wide range of the weight-average molecular weight M_w from 5.90×10^2 to 1.58×10^6 in acetone at 25.0 °C, for $5.90 \times 10^2 \leq M_w \lesssim 2.0 \times 10^5$ in acetonitrile at 44.0 °C (Θ), and for $M_w \gtrsim 2.0 \times 10^5$ in chloroform at 25.0 °C, in nitroethane at 30.0 °C, and in acetonitrile at 47.0, 50.0, and 55.0 °C. It is shown that the observed dependence of A_2 on M_w in the oligomer region may be quantitatively explained by the Yamakawa theory that takes into account the effect of chain ends. The values of the effective excess binary-cluster integrals β_1 and β_2 associated with the chain end beads are then found to be 62 and 910 Å^3, respectively, in acetone at 25.0 °C and −75 and 800 Å^3, respectively, in acetonitrile at Θ by taking the repeat unit as a single bead. The analysis shows that the effect of chain ends remains even for relatively large M_w ($\simeq 10^5$) both in the Θ and good solvents as in the case of atactic polystyrene (a-PS). The results for the true interpenetration function Ψ in A_2 without the effect of chain ends indicate that the two-parameter theory breaks down completely, as found previously for a-PS; the observed Ψ as a function of the cubed radius expansion factor α_S^3 depends separately on M_w and on the excluded-volume strength B. It is then shown that the observed behavior of Ψ and also the remarkable difference in it between a-PMMA and a-PS may be rather satisfactorily explained by the Yamakawa theory that takes into account the effect of chain stiffness on the basis of the helical wormlike chain.

Introduction

Recently, a new theory of the second virial coefficient A_2 that takes into account both effects of chain stiffness and chain ends has been developed by Yamakawa[1] on the basis of the helical wormlike (HW) chain model,[2,3] in order to explain experimental findings inconsistent with the two-parameter-theory prediction.[4] The theory predicts that the chain stiffness has a significant effect on the interpenetration function Ψ appearing in A_2 even for such large molecular weight M that the ratio of the unperturbed mean-square radius of gyration $\langle S^2 \rangle_0$ to M already reaches its coil-limiting value independent of M and also that the effect of chain ends on A_2 becomes appreciable for relatively small M, thereby explaining the observed nonvanishing of A_2 for small M at the Θ temperaure (the temperature at which it vanishes for large M). Corresponding to the theoretical developments, we have made an experimental study of A_2 for atactic oligo- and polystyrenes (a-PS) in Θ and good solvents.[5,6] The results obtained have definitely confirmed the theoretical prediction in all respects. That is, Ψ is not a universal function of the gyration-radius expansion factor α_S but its change with α_S depends separately also on M and on the excluded-volume strength (or solvent power) B. The observed dependence of A_2 on M for relatively small M may be well explained by considering the effects not only of chain stiffness but also of chain ends, the latter remaining significant even at rather large M.

In the present work, we extend the above study to atactic oligo- and poly(methyl methacrylate)s (a-PMMA) with the fraction of racemic diads $f_r = 0.79$, which is remarkably different from a-PS in chain stiffness and local chain conformation. We have already investigated extensively dilute solution properties of the a-PMMA in the Θ state.[7-11] It has then been shown that all the findings obtained for the unperturbed a-PMMA chain in these studies may be well explained consistently by the HW theory, and thus the values of the HW model parameters for a-PMMA have already been established. Subsequently, the gyration- and viscosity-radius expansion factors α_S and α_η for a-PMMA in various good solvents have very recently been investigated.[12] The results have confirmed that the quasi-two-parameter scheme is still valid for both α_S and α_η irrespective of the large differences in chain stiffness, local chain conformation, and solvent condition between a-PMMA and a-PS[13-15] and also polyisobutylene.[14] That is, α_S and α_η also for a-PMMA are functions only of the scaled excluded-volume parameter $\tilde{z}$ defined in the Yamakawa–Stockmayer–Shimada (YSS) theory[16-18] for the perturbed HW chain with excluded volume.

Thus, in this work, we examine separately the effects of chain stiffness and chain ends on A_2 for a-PMMA, making a comparison of the former effect on Ψ with that for a-PS, and then give a theoretical explanation of the difference between the results for the two polymers, which is very remarkable. In this paper, we do not consider the contribution of the ternary-cluster integral to A_2 (and also α_S) as in the previous papers.[5,6,19] The third virial coefficient A_3 of a-PMMA in a Θ solvent is determined simultaneously, but the results are discussed in the following paper.[20]

Experimental Section

Materials. Most of the a-PMMA samples used in this work are the same as those used in the previous studies,[7-12] i.e., the fractions separated by preparative gel permeation chromatography (GPC) or fractional precipitation from the original samples prepared by group-transfer polymerization (GTP). In this study, however, some additional samples were prepared in the same manner as before,[7] i.e., by GTP, followed by separation by preparative GPC or by fractional precipitation. The values of f_r for them were examined by ^{1}H NMR in the same manner as before[7] and were found to coincide with the previous value 0.79 independent of the weight-average molecular weight M_w. Both of the chain ends of all the present samples are hydrogen atoms.

The values of M_w determined from light scattering (LS) measurements are given in Table 1 along with those of the weight-average degree of polymerization x_w and the ratio of M_w to the number-average molecular weight M_n. The samples OM6a, OM8a, OM15, and OM18a are the additional ones, and their M_ws

® Abstract published in *Advance ACS Abstracts*, May 1, 1994.

0024-9297/94/2227-3262$04.50/0

Table 1. Values of M_w, x_w, and M_w/M_n for Atactic Oligo- and Poly(methyl methacrylate)s

sample	M_w	x_w	M_w/M_n
OM6a	5.94×10^2	5.92	1.00
OM8a	7.93×10^2	7.91	1.01
OM12[a]	1.16×10^3	11.6	1.02
OM15	1.50×10^3	15.0	1.03
OM18a	1.83×10^3	18.3	1.05
OM42[a]	4.18×10^3	41.8	1.09
OM51	5.06×10^3	50.6	1.08
OM76	7.55×10^3	75.5	1.08
MM2a	2.02×10^4	202	1.08
MM4	3.40×10^4	340	1.07
MM5	5.04×10^4	504	1.07
MM12	1.18×10^5	1180	1.09
MM20	2.04×10^5	2040	1.08
MM31	3.12×10^5	3120	1.08
Mr4	3.56×10^5	3560	1.07
Mr5	4.82×10^5	4820	1.07
Mr8	7.62×10^5	7620	1.05
Mr8a	7.65×10^5	7650	1.07
Mr16	1.58×10^6	15800	1.08

[a] The results for OM12 and OM42 through Mr16 have been reproduced from ref 12 except for those for OM51, MM5, MM12, Mr4, and Mr8, which have been reproduced from ref 7.

were determined from LS measurements in acetone at 25.0 °C. The values of M_w/M_n indicate that the molecular weight distributions of all the samples are sufficiently narrow for the present purpose.

The solvents acetonitrile, acetone, nitroethane, and chloroform were purified according to standard procedures prior to use.

Light Scattering. LS measurements were carried out to determine A_2 (and also M_w) for the a-PMMA samples with $M_w \lesssim 2.0 \times 10^5$ in acetonitrile at 44.0 °C (Θ) and for the samples with $M_w \lesssim 2.0 \times 10^3$ in acetone at 25.0 °C. Measurements were also made to determine A_2 and the perturbed mean-square radius of gyration $\langle S^2 \rangle$ for three high-molecular-weight samples in acetonitrile at temperatures higher than Θ. A Fica 50 light-scattering photometer was used for all the measurements with vertically polarized incident light of wavelength 436 nm. For a calibration of the apparatus, the intensity of light scattered from pure benzene was measured at 25.0 °C at a scattering angle of 90°, where the Rayleigh ratio $R_{Uu}(90°)$ of pure benzene was taken as 46.5×10^{-6} cm^{-1}. The depolarization ratio ρ_u of pure benzene at 25.0 °C was determined to be 0.41 ± 0.01 by the method of Rubingh and Yu.[21]

While the conventional method was used for solutions of the samples with $M_w > 10^3$, the new procedure previously[22] presented was applied to those of the oligomer samples with $M_w < 10^3$, since the concentration dependence of the density scattering R_d and the optical constant K has significant effects on the determination of A_2 (and also of M_w) in the latter range of M_w. In the analysis of the data obtained by the conventional method we employed the Berry square-root plot[23] as usual and also the Bawn plot[24,25] for the acetonitrile solutions at Θ. The correction for the anisotropic scattering was then applied to the solutions of the samples with $10^3 < M_w \lesssim 4.2 \times 10^3$ (as usual by the use of eq 1 of ref 6).

In order to determine A_2 by the latter method,[22] we measured the reduced total intensity R^*_{Uv} of unpolarized scattered light for vertically polarized incident light, the depolarization ratio ρ_u, the ratio of the isothermal compressibility of a given solution to that of the solvent $\kappa_T/\kappa_{T,0}$, and the refractive index increment $(\partial\tilde{n}/\partial c)_{T,p}$ for the oligomer solutions and also the first two quantities for the solvents. The values of the refractive index $\tilde{n}$ at finite concentrations c, which were required to calculate K, were calculated with the values of $(\partial\tilde{n}/\partial c)_{T,p}$ for each oligomer sample, as described in the Results section. The measurements of R^*_{Uv} were carried out at scattering angles θ ranging from 45 to 135°, and the mean of the values obtained at different θ was adopted as its value, since it must be independent of θ for oligomers. The values of ρ_u were obtained by the same method as employed in the calibration of the apparatus. The refractive index increment $(\partial\tilde{n}/\partial c)_{T,p}$ was determined as a function of c for each oligomer sample by the use of a Shimadzu differential refractometer. The analysis of the LS data obtained was also made by using the Berry square-root plot and the Bawn plot.

The most concentrated solutions of each sample were prepared by continuous stirring at room temperature for ca. 1 day in acetone and at ca. 50 °C for 4 days in acetonitrile. They were optically purified by filtration through a Teflon membrane of pore size 0.45 or 0.10 μm. The solutions of lower concentrations were obtained by successive dilution. The polymer mass concentrations c were calculated from the weight fractions with the densities of the solutions. The densities of the solvents and solutions were measured with a pycnometer of the Lipkin–Davison type.

Isothermal Compressibility. Isothermal compressibility measurements were carried out to determine $\kappa_T/\kappa_{T,0}$ for the oligomer samples with $M_w < 10^3$ in acetonitrile at Θ and in acetone at 25.0 °C. The apparatus and the method of measurements are the same as those described in the previous paper.[6] The ratio $\kappa_T/\kappa_{T,0}$ for each oligomer–solvent system was determined as a function of c and pressure p. The pressure p was varied from 1 to ca. 50 atm.

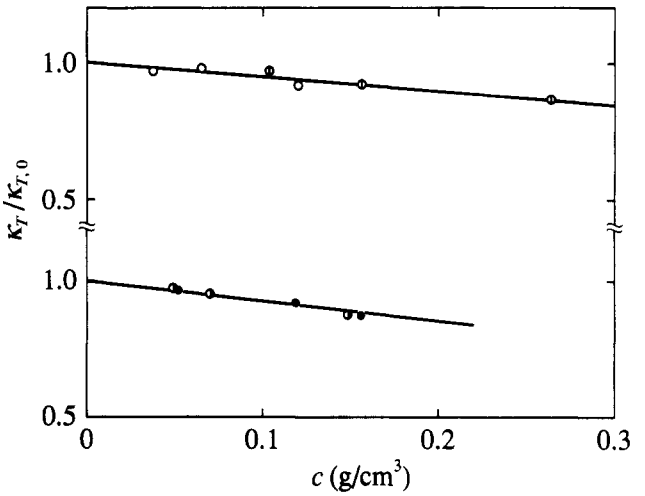

Figure 1. Plots of $\kappa_T/\kappa_{T,0}$ against c for a-PMMA: (○) OM6a; (Φ) OM12 in acetonitrile at 44.0 °C (Θ) (upper part) and (●) OM6a; (◑) OM8a in acetone at 25.0 °C (lower part).

Results

Isothermal Compressibility. In Figure 1, values of $\kappa_T/\kappa_{T,0}$ are plotted against c for the samples OM6a (unfilled circles) and OM12 (circles with bar) in acetonitrile at Θ (upper part), and OM6a (filled circles) and OM8a (right-half-filled circles) in acetone at 25.0 °C (lower part). We note that the ratio $\kappa_T/\kappa_{T,0}$ is independent of p for these oligomers in both solvents within experimental error at any concentration c in the range of p examined as in the case of a-PS,[6] and therefore we adopted the mean of the values obtained at various pressures as its value at 1 atm.

As seen from Figure 1, $\kappa_T/\kappa_{T,0}$ for each sample in each solvent decreases linearly with increasing c. The data points for OM6a and OM12 in acetonitrile form a single straight line, thus leading to the conclusion that $\kappa_T/\kappa_{T,0}$ is independent of x_w for $6 \lesssim x_w \lesssim 12$. It is seen that those for OM6a and OM8a in acetone also form a single straight line. The results may then be represented by the equation linear in c

$$\kappa_T/\kappa_{T,0} = 1 + kc \tag{1}$$

for $c \lesssim 0.3$ g/cm^3 and $c \lesssim 0.2$ g/cm^3 for the acetonitrile and acetone solutions, respectively, as indicated by the straight lines. Here, the values of k have been found to be −0.500 cm^3/g in acetonitrile and −0.730 cm^3/g in acetone at the respective temperatures above.

Light Scattering from Oligo(methyl methacrylate) in Acetone. Figure 2 shows the Berry square-root plots

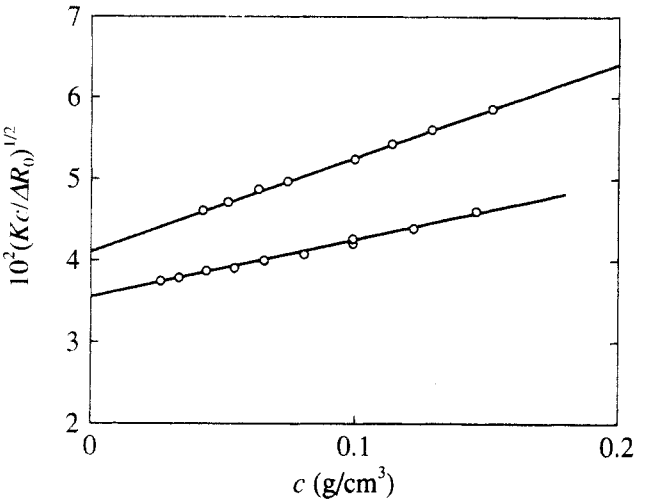

Figure 2. Plots of $(Kc/\Delta R_0)^{1/2}$ against c for the oligomer samples of a-PMMA in acetone at 25.0 °C. The samples are OM6a and OM8a from top to bottom.

of the excess Rayleigh ratio ΔR_0 at $\theta = 0$ against c for the oligomer samples OM6a and OM8a in acetone at 25.0 °C. Here, the values of $(\partial\tilde{n}/\partial c)_{T,p}$ at 436 nm determined to evaluate $\tilde{n}$ and K at finite concentrations c, which are required in the new procedure for the determination of A_2 and M_w of oligomers, have been found to be independent of c for $c \lesssim 0.15$ g/cm^3. The constant values of $(\partial\tilde{n}/\partial c)_{T,p}$ are 0.115_5 and 0.118_0 cm^3/g for OM6a and OM8a in acetone at 25.0 °C, respectively. Thus, for these solutions, the values of $\tilde{n}$ at c in the range of c above may be obtained from the equation

$$\tilde{n} = \tilde{n}_0 + (\partial\tilde{n}/\partial c)_{T,p}c \tag{2}$$

with $\tilde{n}_0 = 1.3647$ for pure acetone at 25.0 °C and the above values of $(\partial\tilde{n}/\partial c)_{T,p}$.

It is seen that the data points for each sample follow a straight line in the range of c studied, from which we can determine A_2 and M_w accurately. Similar results for the Berry square-root plots have also been obtained for the other a-PMMA samples in acetone studied by the conventional method. (The values of $\partial\tilde{n}/\partial c$ for some of them are given in the Appendix of ref 12.)

Light Scattering from a-PMMA in Acetonitrile at Θ. Figure 3 shows the Berry square-root plots of ΔR_0 against c for all the a-PMMA samples studied in acetonitrile at 44.0 °C (Θ). Here, the values of $(\partial\tilde{n}/\partial c)_{T,p}$ at 436 nm have been found to be independent of c for $c \lesssim 0.15$ g/cm^3 as in the case of the acetone solutions. The constant values of $(\partial\tilde{n}/\partial c)_{T,p}$ are 0.126_5 and 0.131_0 cm^3/g for OM6a and OM8a in acetonitrile at Θ, respectively. Thus, for these solutions, the values of $\tilde{n}$ at c in the range of c above may be obtained from eq 2 with these values of $(\partial\tilde{n}/\partial c)_{T,p}$ and $\tilde{n}_0 = 1.340$ for pure acetonitrile at 44.0 °C. For OM12, OM15, and OM18a in acetonitrile at Θ, the values of $\partial\tilde{n}/\partial c$ were 0.138_0, 0.139_0, and 0.139_5 cm^3/g, respectively. (For higher-molecular-weight samples, it is 0.144 cm^3/g.[7]) It is seen from Figure 3 that the data points for each sample follow a curve concave upward, as shown by the solid curve (which represents the values calculated as described below).

Now it can be shown that $Kc/\Delta R_0$ may be expanded as[22]

$$Kc/\Delta R_0 = M_w^{-1} + 2A_2'c + 3A_3'c^2 + \ldots \tag{3}$$

where A_2' and A_3' are the light-scattering second and third virial coefficients, respectively, and are related to the osmotic second and third virial coefficients A_2 and A_3 by

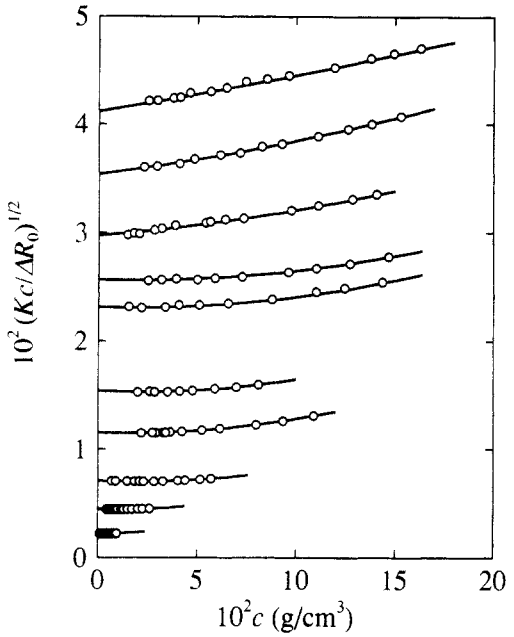

Figure 3. Plots of $(Kc/\Delta R_0)^{1/2}$ against c for a-PMMA in acetonitrile at 44.0 °C (Θ). The samples are OM6a, OM8a, OM12, OM15, OM18a, OM42, OM76, MM2a, MM5, and MM20 from top to bottom.

the equations

$$A_2 = A_2' + \frac{RT\kappa_{T,0}}{2M_w^2} \tag{4}$$

$$A_3 = A_3' + \frac{1}{3M_w}\left(\frac{\partial v_1}{\partial c}\right)_{T,p,0} + \frac{RT\kappa_{T,0}A_2}{M_w} + \frac{RT}{2M_w^2}\left(\frac{\partial \kappa_T}{\partial c}\right)_{T,0} + \frac{(RT)^2}{3M_w^3}\left[\kappa_{T,0}^2 - \left(\frac{\partial \kappa_T}{\partial p}\right)_{T,0}\right] \tag{5}$$

respectively, with R being the gas constant, T the absolute temperature, and v_1 the partial specific volume of the solute (the subscript 0 referring to the pure solvent).

The results in Figure 3 imply that in eq 3, besides the A_2' term, A_3' at least makes a significant contribution to $Kc/\Delta R_0$ as c is increased. It is then difficult to determine A_2' accurately from the plots in this figure. Therefore, we have made the Bawn plots of these data, as indicated for the samples with $M_w < 2.0 \times 10^3$ in Figure 4 and for the samples with $M_w > 4.0 \times 10^3$ in Figure 5, where $S(c_i,c_j)$ is given by

$$S(c_i,c_j) \equiv [(Kc/\Delta R_0)_{c=c_j} - (Kc/\Delta R_0)_{c=c_i}]/(c_j - c_i) \tag{6}$$

$$= 2A_2' + 3A_3'(c_i + c_j) + \ldots \tag{7}$$

with c_i and c_j being two different concentrations. As seen from these figures, the data points for each sample follow a straight line, although those in Figure 4 somewhat scatter. These results indicate that the terms higher than A_3' may be neglected for all samples in the range of c studied. From the straight lines indicated, we have determined A_2' and A_3' for each sample in acetonitrile at Θ. We have then determined M_w for each sample so that the curve of $(Kc/\Delta R_0)^{1/2}$ calculated from eq 3 with these values of M_w, A_2', and A_3' may give a best fit to the data points in Figure 3. The solid curves in Figure 3 represent the values thus calculated. The good fit of each curve to the corresponding data points indicates that M_w, A_2', and A_3' have been determined with sufficient accuracy.

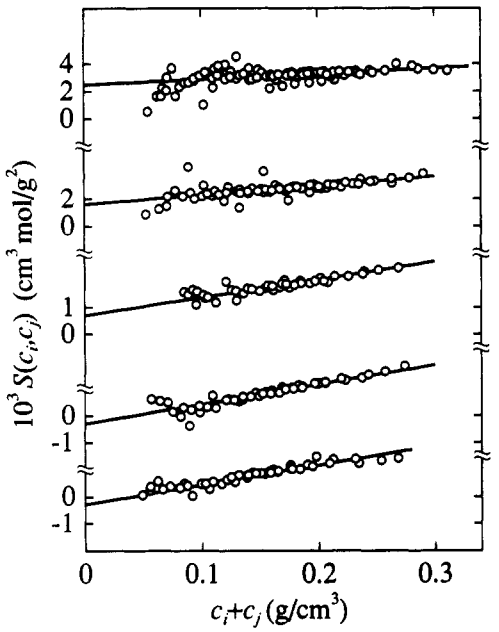

Figure 4. Brawn plots for a-PMMA in acetonitrile at 44.0 °C (Θ). The samples are OM6a, OM8a, OM12, OM15, and OM18a from top to bottom.

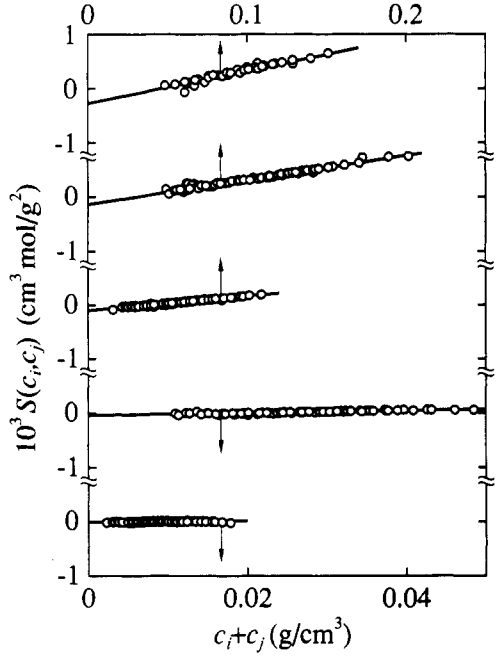

Figure 5. Brawn plots for a-PMMA in acetonitrile at 44.0 °C (Θ). The samples are OM42, OM76, MM2a, MM5, and MM20 from top to bottom.

The values of A_2' and A_3' thus determined may be equated to those of A_2 and A_3, respectively, since the correction terms on the right-hand sides of eqs 4 and 5 are negligibly small compared to A_2' and A_3', respectively, in the present case. For example, for OM6a in acetonitrile at 44.0 °C, we have $\kappa_{T,0} = 1.3 \times 10^{-3}$ cm^3/J, $(\partial v_1/\partial c)_{T,p,0} \simeq 3 \times 10^{-3}$ cm^6/g^2, $(\partial \kappa_T/\partial c)_{T,0} = -6.5 \times 10^{-4}$ cm^6/gJ, and $(\partial \kappa_T/\partial p)_{T,0} \simeq 0$. Then, the correction terms in eq 4 for A_2 and in eq 5 for A_3 are of order 10^{-6} cm^3 mol/g^2 and 10^{-6} cm^6 mol/g^3, respectively, while A_2 and A_3 are of order 10^{-3} cm^3 mol/g^2 and 10^{-3} cm^6 mol/g^3, respectively, as shown below and in the following paper.[20]

Second Virial Coefficient. The values of A_2 determined from LS measurements for all the samples in acetonitrile at 44.0 °C (Θ) and in the three good solvents acetone at 25.0 °C, nitroethane at 30.0 °C, and chloroform at 25.0 °C are summarized in Table 2 along with those of M_w, and those of A_2 for the three samples in acetonitrile at various temperatures are given in Table 3 along with the data for $\langle S^2 \rangle^{1/2}$. (The values of A_3 in acetonitrile at Θ are reported in the following paper.[20]) Table 2 also includes the results obtained previously[7,12] for M_w and A_2.

In Figure 6, the data for A_2 in acetonitrile at 44.0 °C (Θ) are plotted against log M_w, since it has negative values for $1.5 \times 10^3 \lesssim M_w \lesssim 2.0 \times 10^5$. The solid curve connects the data points smoothly. It is rather striking to see that, as M_w is increased, A_2 in acetonitrile at Θ first decreases steeply from positive to negative values, then passes through a minimum, and finally increases to zero. (We note that the previous results from small-angle X-ray scattering measurements[7] given in Figure 6 of ref 1 are less accurate and do not exhibit the minimum.) The value of M_w above which A_2 at Θ becomes negligibly small (smaller than 5×10^{-6}) is ca. 2.0×10^5.

Figure 7 shows double-logarithmic plots of A_2 against M_w in chloroform at 25.0 °C (top-half-filled circles), in nitroethane at 30.0 °C (bottom-half-filled circles), in acetone at 25.0 °C (unfilled circles), and in acetonitrile at 55.0 °C (right-half-filled circles), 50.0 °C (circles with bar), and 47.0 °C (left-half-filled circles). The solid curves connect the data points smoothly. It is seen that A_2 in acetone at 25.0 °C also exhibits an upswing with decreasing M_w for small M_w. This result is consistent with the literature data obtained by Springer et al.[26] from vapor pressure osmometry for methyl methacrylate oligomers in the same solvent, although their data exhibit a sharp decrease with decreasing M_w for $M_w < 300$. However, its direct comparison with our data may be inappropriate since the terminal groups of their samples are unknown.

The sharp increases in A_2 in acetonitrile at Θ and in acetone at 25.0 °C for small M_w are similar to its behavior observed for a-PS in cyclohexane at Θ and in toluene at 15.0 °C.[6] Thus this behavior of A_2 of a-PMMA may be regarded as arising from the effect of chain ends as in the case of a-PS. It must then be emphasized that the present results for the acetonitrile solutions at Θ cannot be explained by the theory of, for instance, Cherayil et al.[27] that takes into account the contribution of the ternary-cluster integral,[28] since it can only predict a monotonical decrease (or increase) in A_2 at Θ with decreasing M.

Discussion

HW Theory. For convenience, we begin by outlining the Yamakawa HW theory[1] of A_2. It considers also the effect of chain ends on the basis of the HW touched-bead model. It is such that $n + 1$ beads are arrayed with spacing a between them along the contour of total length $L = na$, where the $n - 1$ intermediate beads are identical and the two end beads are different from the intermediate ones and also from each other in species. Identical excluded-volume interactions are expressed in terms of the conventional binary-cluster integral β, while two kinds of *effective excess* binary-cluster integrals, β_1 and β_2, are necessary to express interactions between unlike (and like end) beads, β_1 being associated with one end bead and β_2 with two end ones. The HW model itself[2,3] is defined in terms of the three basic model parameters: the constant differential-geometrical curvature κ_0 and torsion τ_0 of its characteristic helix and the static stiffness parameter λ^{-1}.

According to the theory,[1] A_2 in general may be written in the form

$$A_2 = A_2^{(HW)} + A_2^{(E)} \tag{8}$$

where $A_2^{(HW)}$ is that part of A_2 without the effect of chain

Table 2. Results of Light-Scattering Measurements on Atactic Oligo- and Poly(methyl methacrylate)s in Acetonitrile at 44.0 °C (Θ) and in Good Solvents

	acetonitrile at 44.0 °C		acetone at 25.0 °C		nitroethane at 30.0 °C		chloroform at 25.0 °C	
sample	$10^{-4}M_w$	10^4A_2(cm³ mol/g²)	$10^{-4}M_w$	10^4A_2(cm³ mol/g²)	$10^{-4}M_w$	10^4A_2(cm³ mol/g²)	$10^{-4}M_w$	10^4A_2(cm³ mol/g²)
OM6a	0.0590	12.5	0.0594	47.3				
OM8a	0.0800	8.0	0.0793	25.0				
OM12[a]	0.113	3.5	0.116	17.6				
OM15	0.152	−1.5	0.150	10.8				
OM18a	0.187	−1.4	0.183	10.6				
OM42[a]	0.420	−1.40	0.418	5.58				
OM51			0.506	4.53				
OM76	0.750	−0.68	0.755	4.58				
MM2a	2.00	−0.50	2.02	3.54				
MM4	3.53		3.40	3.27				
MM5	5.02	−0.20	5.04	2.71				
MM12	11.9		11.8	2.29				
MM20	20.7	−0.04	20.4	1.91	19.8	3.32	20.5	5.66
MM31	32.2		31.2	1.75	30.6	2.97	31.1	5.06
Mr4	36.1		35.6	1.72				
Mr5	49.8		48.2	1.60	47.9	2.61	48.6	4.39
Mr8	75.8		76.2	1.28				
Mr8a	79.0		76.5	1.39	76.3	2.32	77.8	3.91
Mr16	157		158	1.25	155	1.99	161	3.31

[a] M_ws for OM51, MM5, MM12, Mr4, and Mr8 have been reproduced from ref 7, and those for the other samples from OM42 through Mr16 and for OM12, from ref 12. The values of A_2 for all of them in the three good solvents had been determined there, although not reported.

Table 3. Results of Light-Scattering Measurements on Atactic Poly(methyl methacrylate)s in Acetonitrile at 47.0, 50.0, and 55.0 °C

		47.0 °C		50.0 °C		55.0 °C	
sample	$10^{-4}M_w$	$\langle S^2\rangle^{1/2}$ (Å)	10^4A_2 (cm³ mol/g²)	$\langle S^2\rangle^{1/2}$ (Å)	10^4A_2 (cm³ mol/g²)	$\langle S^2\rangle^{1/2}$ (Å)	10^4A_2 (cm³ mol/g²)
MM31	32.2	145	0.100	146	0.175	148	0.256
Mr5	49.8	179	0.114	182	0.184	185	0.279
Mr8a	79.0	229	0.107	232	0.177	236	0.292

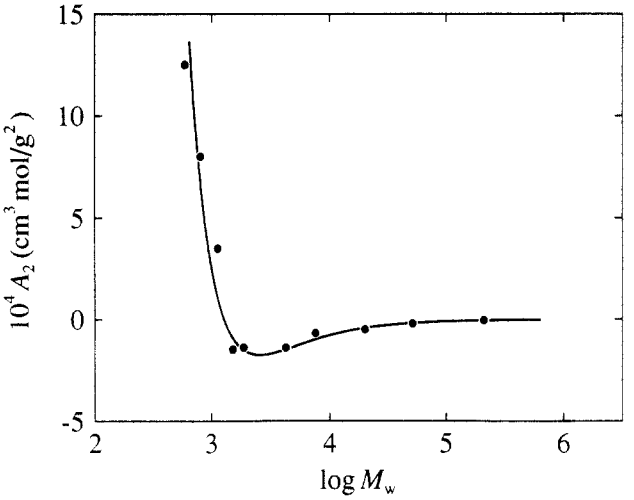

Figure 6. Plots of A_2 against log M_w for a-PMMA in acetonitrile at 44.0 °C (Θ). The solid curve connects the data points smoothly.

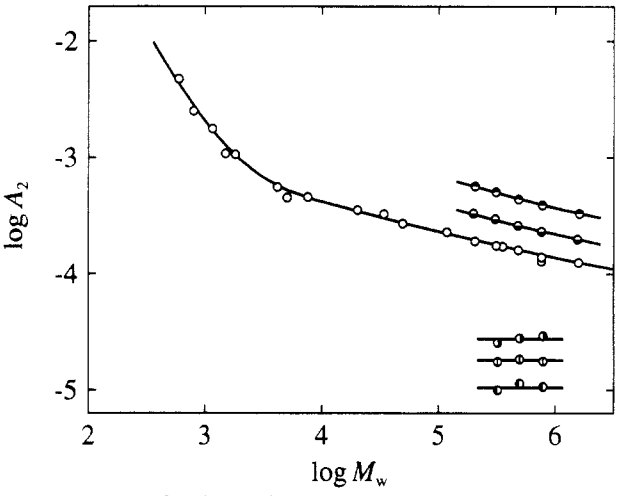

Figure 7. Double-logarithmic plots of A_2 against M_w for a-PMMA: (◓) in chloroform at 25.0 °C; (◒) in nitroethane at 30.0 °C; (○) in acetone at 25.0 °C; (◑) in acetonitrile at 55.0 °C; (◔) in acetonitrile at 50.0 °C; (◐) in acetonitrile at 47.0 °C. The solid curves connect the data points smoothly.

ends which vanishes at Θ, or A_2 for the (fictitious) chain composed of $n+1$ identical beads, and $A_2^{(E)}$ represents the contribution of the effect of chain ends to A_2. The first term $A_2^{(HW)}$ may be written as

$$A_2^{(HW)} = (N_A c_\infty^{3/2} L^2 B/2M^2)h \tag{9}$$

where N_A is Avogadro's number, and the constant c_∞ and the excluded-volume strength B are given by

$$c_\infty = \lim_{\lambda L\to\infty} (6\lambda\langle S^2\rangle_0/L)$$

$$= \frac{4 + (\lambda^{-1}\tau_0)^2}{4 + (\lambda^{-1}\kappa_0)^2 + (\lambda^{-1}\tau_0)^2} \tag{10}$$

and

$$B = \beta/a^2 c_\infty^{3/2} \tag{11}$$

The h function is given by

$$h(\hat{z}) = (1 + 7.74\hat{z} + 52.3\hat{z}^{27/10})^{-10/27} \tag{12}$$

with

$$\hat{z} = \tilde{z}/\alpha_S^3 \tag{13}$$

In eq 13, $\tilde{z}$ is the intermolecular scaled excluded-volume parameter defined by

$$\tilde{\tilde{z}} = [Q(\lambda L)/2.865]z \quad (14)$$

where the conventional excluded-volume parameter z is defined by

$$z = (3/2\pi)^{3/2}(\lambda B)(\lambda L)^{1/2} \quad (15)$$

and Q is a function only of λL for ordinary flexible polymers and given by eq 19 of ref 1 for $\lambda L \gtrsim 1$.

In the YSS theory,[16-18] α_S^2 ($=\langle S^2\rangle/\langle S^2\rangle_0$) is assumed to be a function only of the intramolecular scaled excluded-volume parameter $\tilde{z}$ defined by

$$\tilde{z} = (3/4)K(\lambda L)z \quad (16)$$

where K is a function only of λL and given by eq 9 of ref 1, and the Domb–Barrett equation[29] for α_S^2 is adopted with $\tilde{z}$ in place of z,

$$\alpha_S^2 = [1 + 10\tilde{z} + (70\pi/9 + 10/3)\tilde{z}^2 + 8\pi^{3/2}\tilde{z}^3]^{2/15}[0.933 + 0.067\exp(-0.85\tilde{z} - 1.39\tilde{z}^2)] \quad (17)$$

Thus, note that h is a function of $\tilde{z}$ and $\tilde{\tilde{z}}$ and that eq 9 for $A_2^{(HW)}$ is valid for $\lambda L \gtrsim 1$, and we may put $h = 1$ approximately for $\lambda L \lesssim 1$. Recall that L is related to M by the equation

$$L = M/M_L \quad (18)$$

with M_L the shift factor as defined as the molecular weight per unit contour length.

Now the second term $A_2^{(E)}$ in eq 8 may be written in the form

$$A_2^{(E)} = a_1M^{-1} + a_2M^{-2} \quad (19)$$

where

$$a_1 = 2N_A\beta_1/M_0 \quad (20)$$

$$a_2 = 2N_A\Delta\beta_2$$

with M_0 the molecular weight of the bead and with

$$\Delta\beta_2 = \beta_2 - 2\beta_1 \quad (21)$$

The effective excess binary-cluster integrals β_1 and β_2 are explicitly defined in eqs 22 of ref 1.

Effects of Chain Ends. We analyze the data for A_2 in Tables 2 and 3 by the use of the theory above to first examine the effect of chain ends, as done previously[6] for a-PS, for convenience. In Figure 8, the values of $A_2^{(E)}M_w$ are plotted against M_w^{-1} on the basis of eq 19 for all the samples in acetonitrile at Θ (filled circles) and for the samples with $M_w \lesssim 7.5 \times 10^3$ in acetone at 25.0 °C (unfilled circles) in order to determine a_1 and a_2 (and hence β_1 and β_2) from the intercept and slope, respectively. Here, we have put $A_2 = A_2^{(E)}$ for the acetonitrile solutions at Θ, since then $A_2^{(HW)} = 0$ ($\beta = 0$). On the other hand, for the acetone solutions, we have obtained the values of $A_2^{(E)}$ by subtracting $A_2^{(HW)}$ from A_2, where we have calculated $A_2^{(HW)}$ for each sample from eqs 9–18 (assuming that $h = 1$ for $\lambda L \lesssim 1$) with the values of the HW model parameters determined previously[7] from $\langle S^2\rangle_0$, i.e., $\lambda^{-1}\kappa_0 = 4.0$, $\lambda^{-1}\tau_0 = 1.1$, $\lambda^{-1} = 57.9$ Å, and $M_L = 36.3$ Å^{-1}, and the value of B (or λB) determined[12] from α_S, i.e., $\lambda B = 0.22$.

It is seen that the data points for each solvent system can be fitted by a straight line, although they somewhat scatter. The results confirm the validity of eq 19, which predicts that the nonvanishing of A_2 at Θ and the upswing of A_2 for small M in the good solvent arise from the effect of chain ends. From the straight lines, a_1 and a_2 are found to be −0.90 cm^3/g and 1150 cm^3/mol, respectively, for the acetonitrile solutions at Θ and 0.75 cm^3/g and 950 cm^3/mol, respectively, for the acetone solutions. Then, β_1 and β_2 are determined to be −75 and 800 Å^3, respectively, in acetonitrile at Θ, and 62 and 910 Å^3, respectively, in acetone at 25.0°C, from eqs 20 and 21 with the above values of a_1 and a_2 by taking the repeat unit as a single bead (M_0 = 100). These values of β_1 and β_2 are of the order of magnitude comparable to those obtained for a-PS in cyclohexane at Θ and in toluene at 15.0 °C[6] and may be regarded as reasonable as the effective excess binary-cluster integrals associated with the chain end beads compared to those for small molecules.[30]

In Figure 9, the theoretical values of A_2 calculated with the values of all the parameters determined above are compared with the observed ones for the acetonitrile solutions at Θ (filled circles) and for the acetone solutions (unfilled circles). For the latter system, the solid curve represents the complete theoretical values, while the chain curve represents the values calculated with $h = 1$ for $\lambda L \lesssim 1$. The dashed and dotted curves indicate the calculated contributions of $A_2^{(HW)}$ and $A_2^{(E)}$ to A_2, respectively, in this

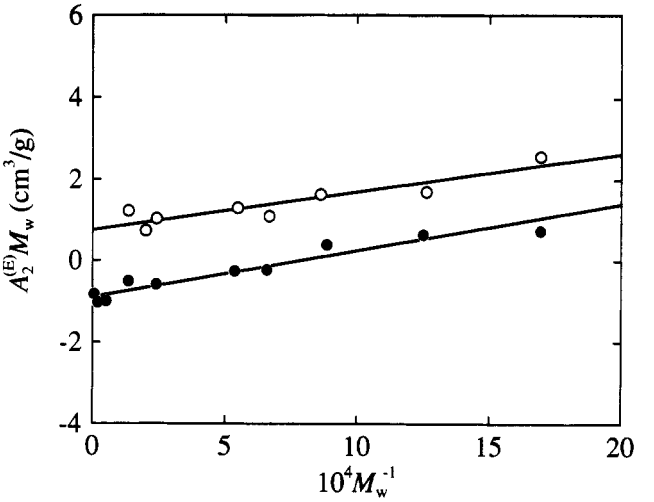

Figure 8. Plots of $A_2^{(E)}M_w$ against M_w^{-1} for a-PMMA. The symbols have the the same meaning as those in Figures 6 and 7.

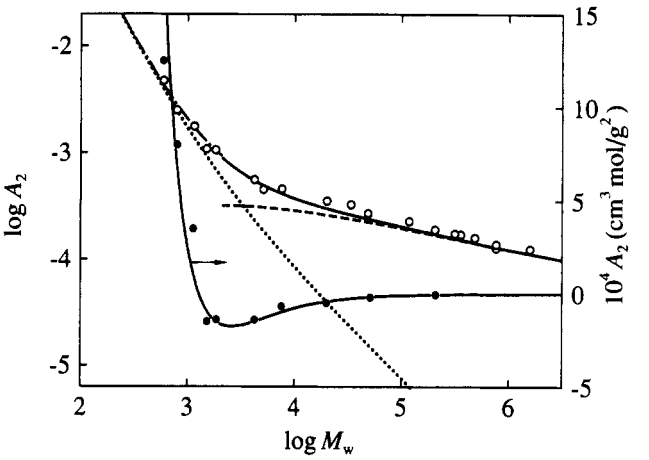

Figure 9. Comparison between the theoretical and observed values of A_2 as a function of M_w for a-PMMA in acetonitrile at 44.0 °C (Θ) and in acetone at 25.0 °C. The solid and chain curves represent the theoretical values of A_2, and the dashed and dotted curves, those of $A_2^{(HW)}$ and $A_2^{(E)}$, respectively (see the text). The symbols have the same meaning as those in Figures 6 and 7.

Table 4. Values of α_S^3 and Ψ of Oligo- and Poly(methyl methacrylate)s in Acetone at 25.0 °C, in Nitroethane at 30.0 °C, and in Chloroform at 25.0 °C

	acetone at 25.0 °C			nitroethane at 30.0 °C		chloroform at 25.0 °C	
sample	α_S^3	Ψ_{ap}	Ψ	α_S^3	Ψ	α_S^3	Ψ
OM6a	1.0	1.50	0.245				
OM8a	1.0	0.592	0.010				
OM12	1.0	0.370	0.086				
OM15	1.0	0.209	0.031				
OM18a	1.0	0.201	0.069				
OM42	1.0	0.147	0.085				
OM51	1.0	0.128	0.076				
OM76	1.06	0.159	0.119				
MM2a	1.15	0.191	0.170				
MM4	1.36	0.187	0.174				
MM5	1.47	0.191	0.180				
MM20	1.78	0.216	0.212	2.59	0.242	3.95	0.291
MM31	1.92	0.222	0.219	2.72	0.252	4.46	0.275
Mr5	2.18	0.222	0.220	3.28	0.239	4.95	0.273
Mr8a	2.43	0.221	0.219	3.75	0.239	5.91	0.266
Mr16	3.02	0.233	0.232	4.92	0.219	7.96	0.244

system. (Note that, for the former system, $A_2 = A_2^{(E)}$, whose values have been calculated from eq 19.)

It is interesting to see that the theory well explains the rather complicated molecular weight dependence of A_2 in acetonitrile at Θ. There is also seen to be good agreement between the theory and experiment for the acetone solutions. Strictly, however, for this system, the theoretical values seem to be slightly smaller than the observed ones for $M_w > 10^4$. This may be regarded as arising from the fact that the theory underestimates somewhat the h (or Ψ) function in the intermediate range of z, as mentioned previously.[6] The literature data obtained by Springer et al.[26] for the same system have been analyzed in a similar way, as shown in the Appendix. The theory is also seen to explain their results with sufficient success.

It is seen from Figure 9 that the contribution of $A_2^{(E)}$ to A_2, i.e., the effect of chain ends, remains significant at least up to $M_w = 10^5$ in both systems. These findings are consistent with the previous results for a-PS in cyclohexane at Θ and in toluene at 15.0 °C.

Interpenetration Function. Next we proceed to examine the effect of chain stiffness on the interpenetration function. We define as before[6] the *apparent* interpenetration function Ψ_{ap} from the whole A_2 with the contribution $A_2^{(E)}$ of the effect of chain ends by the equation

$$\Psi_{ap} = A_2 M^2/4\pi^{3/2}N_A\langle S^2\rangle^{3/2} \quad (22)$$

As is evident from its original physical meaning,[4] the true interpenetration function Ψ must then be redefined by

$$\Psi = A_2^{(HW)} M^2/4\pi^{3/2}N_A\langle S^2\rangle^{3/2} \quad (23)$$

and it is given from eqs 9 and 23 by

$$\Psi = (6\lambda\langle S^2\rangle_0/c_\infty L)^{-3/2}(z/\alpha_S^3)h \quad (24)$$

In Table 4 are listed the values of Ψ_{ap} and Ψ for a-PMMA in acetone at 25.0 °C and those of Ψ in nitroethane at 30.0 °C and in chloroform at 25.0 °C, along with those[12] of α_S^3. Here, we have calculated Ψ_{ap} and Ψ from eqs 22 and 23 with eq 8 with the values of A_2 and M_w in Table 2 and those of $\langle S^2\rangle^{1/2}$ given in Table 2 of ref 12 for the respective samples in the respective solvents. We note that $\langle S^2\rangle$ for the samples OM8a, OM12, OM15, and OM51 in acetone have been calculated from the curve shown in Figure 1 of ref 12 (see also Figure 13a below). For the acetone solutions, we have obtained the values of $A_2^{(HW)}$ from A_2 by subtraction of $A_2^{(E)}$ calculated from eq 14 with the above values of a_1 and a_2. Since $A_2^{(E)}$ is negligibly small for $M_w \gtrsim 10^5$, Ψ ($=\Psi_{ap}$) for a-PMMA in nitroethane and in chloroform may be directly calculated from eq 22 with the respective experimental values of A_2. The values of Ψ ($=\Psi_{ap}$) for a-PMMA in acetonitrile at various temperatures have also been calculated from eq 22 with the values of A_2, $\langle S^2\rangle^{1/2}$, and M_w in Table 3 and are listed in Table 5. From a comparison between Ψ_{ap} and Ψ for a-PMMA in acetone, the contribution of $A_2^{(E)}$ to Ψ_{ap} is seen to be negligibly small in the ordinary range of M_w, i.e., for $M_w \gtrsim 2 \times 10^5$, but becomes progressively large as M_w is decreased.

Table 5. Values of α_S^3 and Ψ of Oligo- and Poly(methyl methacrylate)s in Acetonitrile at 47.0, 50.0, and 55.0 °C

	47.0 °C		50.0 °C		55.0 °C	
sample	α_S^3	Ψ	α_S^3	Ψ	α_S^3	Ψ
MM31	1.02	0.025	1.04	0.043	1.07	0.065
Mr5	1.01	0.037	1.06	0.056	1.10	0.082
Mr8a	1.03	0.048	1.08	0.068	1.13	0.106

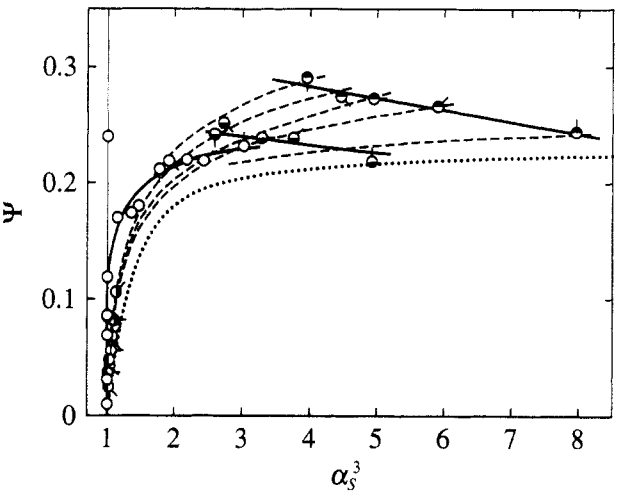

Figure 10. Plots of Ψ against α_S^3 for a-PMMA. Various types of circles indicate different solvent conditions with the same meaning as in Figure 7. Various directions of pips indicate different values of M_w of the five highest-molecular-weight samples: pip up, Mr16; pip right-up, Mr8a; pip right, Mr5; pip right-down, MM31; pip down, MM20. The solid and dashed curves connect smoothly the data points at fixed B (solvent condition) and M_w, respectively. The dotted curve represents the two-parameter-theory values.

All the data for Ψ thus determined are plotted against α_S^3 in Figure 10. Here, the symbols have the same meaning as those in Figure 7; various types of circles indicate different solvent conditions (different excluded-volume strengths B), and various directions of pips attached to them indicate different values of M_w of the five highest-molecular-weight samples. The solid curves connect smoothly the data points for different M_w at fixed B, while for those five samples the dashed curves connect smoothly the data points for different B at fixed M_w. The dotted curve represents the two-parameter-theory (coil-limiting) values calculated from[1,5,6]

$$\Psi = (z/\alpha_S^3)h \quad (25)$$

with $\tilde{z} = \tilde{z} = z$.

As found previously[5] for a-PS, the present results for Ψ for a-PMMA again indicate that Ψ as a function of α_S^3 depends separately on M_w and on B, which is inconsistent with the two-parameter-theory prediction. It increases

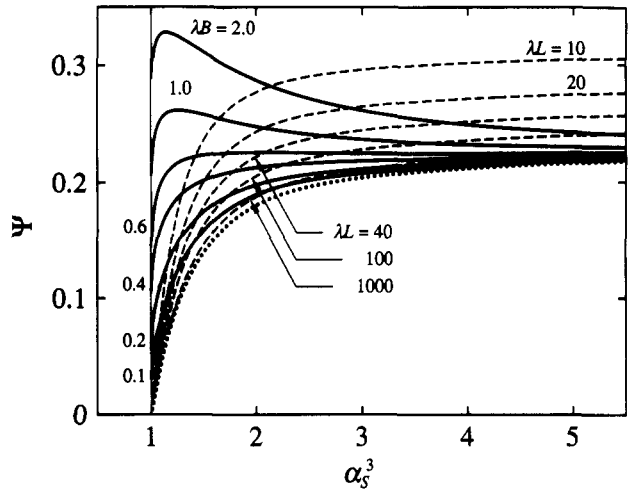

Figure 11. Plots of the theoretical Ψ against α_S^3 for a-PMMA. The solid and dashed curves represent the values at fixed λB and λL, respectively. The dotted curve represents the two-parameter-theory values.

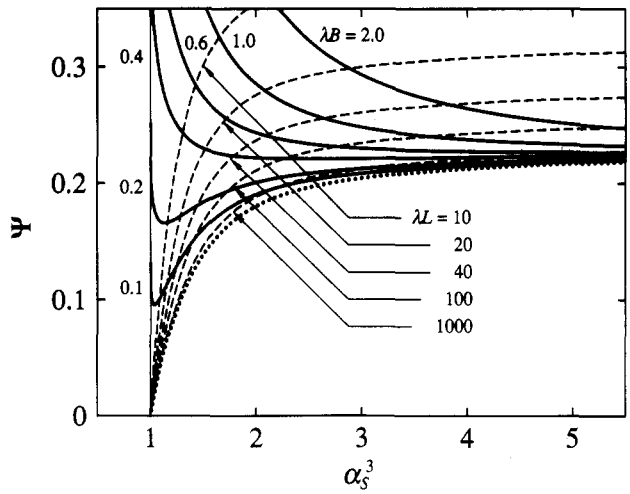

Figure 12. Plots of the theoretical Ψ against α_S^3 for a-PS. The solid and dashed curves represent the values at fixed λB and λL, respectively. The dotted curve represents the two-parameter-theory values.

with decreasing α_S^3 in chloroform and in nitroethane, deviating remarkably upward from the dotted curve. Although Ψ in acetone decreases with decreasing α_S^3 as the two-parameter theory predicts (except for OM6a with M_w = 594), it deviates systematically upward from the latter prediction. As shown by the dashed curves, Ψ increase more rapidly than the two-parameter-theory prediction and with larger slopes for smaller M_w as α_S^3 (or B) is increased at fixed M_w.

All these features of the behavior of Ψ as a function of α_S^3 for a-PMMA may be well explained by the Yamakawa HW theory[1] as arising from the effect of chain stiffness, as in the case of a-PS.[5] The present findings for a-PMMA are qualitatively consistent with the previous ones for a-PS. Quantitatively, however, there are significant differences between them. Before proceeding to make such a comparison between the observed results for a-PMMA and a-PS, it is convenient to present the theoretical results for Ψ for the two polymers and discuss the predicted difference between them. In Figure 11 are shown values of Ψ for a-PMMA calculated from eq 24 with eqs 10–17 and eq 1 of ref 1 for $\langle S^2\rangle_0$ with the values of the parameters given above. The corresponding values for a-PS similarly calculated (see ref 5) are shown in Figure 12 (see also Figure 1 of ref 5). In these figures, the solid curves represent the values for the case in which λL (or M) is changed at fixed λB, while the dashed curves represent the values for the case in which λB is changed at fixed λL (or M), and the dotted curves indicate the two-parameter-theory prediction. The left end of each solid curve at $\alpha_S^3 = 1$ corresponds to $\lambda L = 1$.

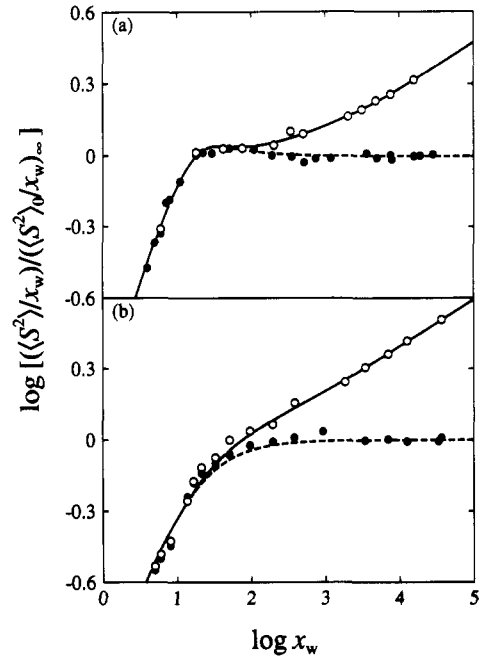

Figure 13. Double-logarithmic plots of $(\langle S^2\rangle/x_w)/(\langle S^2\rangle_0/x_w)_\infty$ against x_w. (a) a-PMMA: (○) in acetone at 25.0 °C; (●) in acetonitrile at 44.0 °C (Θ). (b) a-PS: (○) in toluene at 15.0 °C; (●) in cyclohexane at 34.5 °C (Θ). The solid and dashed curves represent the YSS theory values with $\lambda B \neq 0$ and $\lambda B = 0$, respectively.

Figures 11 and 12 show that, for finite λB and λL, Ψ always deviates upward from the two-parameter-theory prediction, which is obtained as the asymptotic limit of $\lambda B \to 0$ or $\lambda L \to \infty$, in common for a-PMMA and for a-PS. However, there are significant differences between the theoretical values for the two polymers. They are summarized as follows: (1) when compared at the same α_S^3, Ψ at fixed λB and λL deviates from the two-parameter-theory values less appreciably for a-PMMA than for a-PS, and (2) as α_S^3 is decreased for small α_S^3 close to unity, Ψ at fixed λB for a-PMMA decreases monotonically or after passing through a maximum toward a finite value at λL = 1, while for a-PS it increases monotonically or after passing through a minimum. In particular, the second difference may be explained by considering the large differences between the two polymers in chain stiffness and local chain conformation, which are reflected in the molecular weight dependence of $\langle S^2\rangle_0$ and $\langle S^2\rangle$.

It is then helpful to reproduce the double-logarithmic plots of $(\langle S^2\rangle/x_w)/(\langle S^2\rangle_0/x_w)_\infty$ against x_w for a-PMMA in acetone at 25.0 °C (unfilled circles) and in acetonitrile at Θ (filled circles) in Figure 13a and for a-PS in toluene at 15.0 °C (unfilled circles) and in cyclohexane at Θ (filled circles) in Figure 13b from refs 12 and 13, respectively. In these figures, the solid and dashed curves represent the YSS theory values with $\lambda B \neq 0$ and $\lambda B = 0$, respectively. In the case of a-PS, $\langle S^2\rangle/x_w$ in toluene decreases to approach $\langle S^2\rangle_0/x_w$ rather slowly with decreasing x_w, so that α_S becomes unity at a value of x_w for which $\langle S^2\rangle/x_w$ or $\langle S^2\rangle_0/x_w$ is appreciably lower than the coil-limiting value $(\langle S^2\rangle_0/x_w)_\infty$ of the latter, and thus Ψ is large at $\alpha_S^3 = 1$, as seen from eq 24. In contrast to this, for a-PMMA in acetone α_S becomes unity at a value of x_w at which $\langle S^2\rangle_0/x_w$ has nearly a maximum value, and, moreover, in the

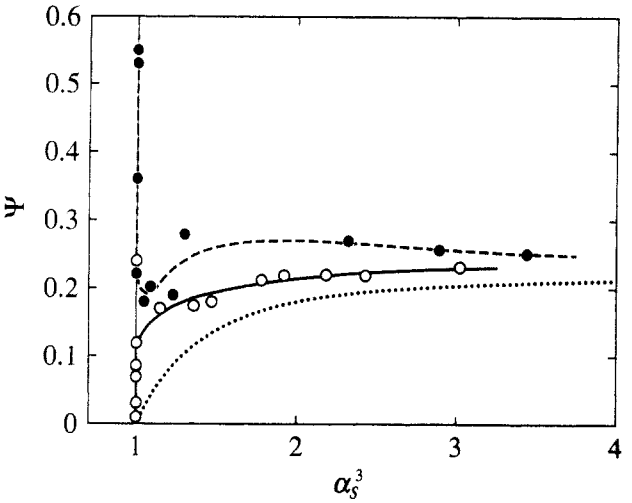

Figure 14. Plots of Ψ against α_S^3: (○) a-PMMA in acetone at 25.0 °C; (●) a-PS in toluene at 15.0 °C. The solid and dashed curves connect smoothly the data points, and the dotted curve represents the two-parameter-theory values.

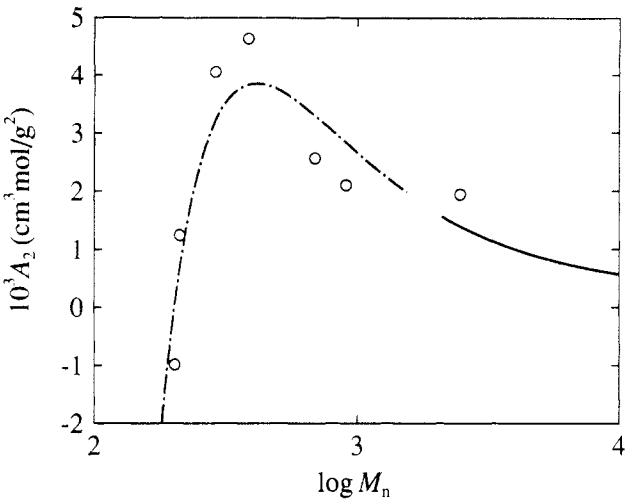

Figure 15. Comparison between the theoretical and observed values of A_2 as a function of M_n for a-PMMA in acetone at 25.0 °C: (○) observed. The solid and chain curves represent the theoretical values (see the text).

range of x_w corresponding to $\alpha_S \geq 1$, $\langle S^2\rangle/x_w$ decreases following a curve significantly concave upward with decreasing x_w. The difference between a-PMMA and a-PS in the way of variation of $\langle S^2\rangle/x_w$ with x_w may explain the difference in the dependence of Ψ on λL, i.e., the variation of Ψ with α_S^3 at fixed λB as shown in Figures 11 and 12. Recall that the salient behavior of $\langle S^2\rangle_0/x_w$ for a-PMMA arises from the strong helical nature and large stiffness of its chain, as discussed previously.[7]

Finally, in Figure 14 are compared the present experimental values of Ψ as a function of α_S^3 for a-PMMA in acetone at 25.0 °C (unfilled circles) with the previous ones[6] for a-PS in toluene at 15.0 °C (filled circles), corresponding to Figure 13. The solid and dashed curves connect smoothly the data points for the former and the latter, respectively, and the dotted curve represents the two-parameter-theory values. The reason we have chosen these two systems for comparison is that the values of λB for them are 0.22 and 0.26, respectively, and are close to each other. It is seen that the variations of Ψ with α_S^3 (or M_w) for a-PMMA and a-PS are in sharp contrast. As α_S^3 is decreased, Ψ decreases monotonically for a-PMMA (except for OM6a with $M_w = 594$), while it increases steeply after passing through a minimum for small α_S^3 for a-PS. As shown in Figures 11 and 12, the theory may explain satisfactorily this large difference in the behavior of Ψ between a-PMMA and a-PS (at the same λB), although there is no complete quantitative agreement between theory and experiment.

Conclusion

In this work, we have determined A_2 for a-PMMA in the Θ and good solvents over a wide range of M_w, including the oligomer region, from light-scattering measurements. It has been found that, as M_w is decreased, A_2 in acetonitrile at Θ first decreases steeply from positive to negative values, then passes through a minimum, and finally increases to zero and that A_2 in acetone at 25.0 °C steeply increases with decreasing M_w for $M_w \lesssim 2.0 \times 10^3$. These results may be quantitatively explained by the Yamakawa theory[1] that takes into account the effect of chain ends, thereby yielding reasonable values of the effective excess binary-cluster integrals β_1 and β_2 associated with the chain end beads. The analysis has shown that the effect of chain ends on A_2, i.e., $A_2^{(E)}$, remains appreciable even at rather large M_w ($\simeq 10^5$) both in the Θ and good solvents, as in the case of a-PS.[6]

As for the interpenetration function Ψ, it has been found that, as α_S^3 (or M_w) is decreased, the true Ψ without the effect of chain ends increases in the extremely good solvents, chloroform and nitroethane, and decreases in acetone, all the data in these solvents deviating significantly upward from the two-parameter-theory prediction. Also, in contradiction to the two-parameter-theory prediction, Ψ at fixed M_w increases with increasing reduced excluded-volume strength λB (or α_S^3) following different curves dependent on M_w. All these salient features of the behavior of Ψ as a function of α_S^3 for a-PMMA are qualitatively in good agreement with those found previously[5] for a-PS. Quantitatively, however, there are significant differences between the results for the two polymers; e.g., as α_S^3 is decreased, Ψ decreases monotonically for a-PMMA in acetone at 25.0 °C, while it increases steeply after passing through a minimum for a-PS in toluene at 15.0 °C, despite the fact that the values of λB for these two polymer–solvent systems are approximately equal to each other. All these results for Ψ as a function of α_S^3, including the difference in it between the two polymers, may be rather satisfactorily explained by the Yamakawa theory[1] that takes into account the effect of chain stiffness. In particular, the above behavior of Ψ for a-PMMA in acetone may be explained as arising from the strong helical nature and large stiffness of its chain.

Appendix. Analysis of Literature Data for Oligomers

Following the procedure described in the text, we have analyzed the literature data obtained by Springer et al.[26] for A_2 from vapor pressure osmometry for methyl methacrylate oligomers in acetone at 25.0 °C. (We note that the chemical structures of the end groups of their samples are unknown, as already mentioned.) In the calculation of $A_2^{(HW)}$, we have assumed that $h = 1$ for $\lambda L \lesssim 1$ and adopted the same values of the HW model parameters and λB as those given in the text. The values obtained for β_1 and β_2 per repeat unit are 240 and −17 Å^3, respectively, and are different from those determined in the present work for a-PMMA in the same solvent. This difference may possibly be due to that in the end groups between our and their oligomer samples.

Their data for A_2 (unfilled circles) are plotted against $\log M_n$ in Figure 15, where the solid and chain curves have the same meaning as those in Figure 9. It is seen that the

theory may explain satisfactorily the observation that, as M_n is decreased, A_2 first increases, then passes through a maximum at $M_n \simeq 380$, and finally decreases steeply to a negative value for the dimer.

References and Notes

(1) Yamakawa, H. *Macromolecules* **1992**, *25*, 1912.
(2) Yamakawa, H. *Annu. Rev. Phys. Chem.* **1984**, *35*, 23.
(3) Yamakawa, H. In *Molecular Conformation and Dynamics of Macromolecules in Condensed Systems*; Nagasawa, M., Ed.; Elsevier: Amsterdam, The Netherlands, 1988; p 21.
(4) Yamakawa, H. *Modern Theory of Polymer Solutions*; Harper & Row: New York, 1971.
(5) Yamakawa, H.; Abe, F.; Einaga, Y. *Macromolecules* **1993**, *26*, 1898.
(6) Einaga, Y.; Abe, F.; Yamakawa, H. *Macromolecules* **1993**, *26*, 6243.
(7) Tamai, Y.; Konishi, T.; Einaga, Y.; Fujii, M.; Yamakawa, H. *Macromolecules* **1990**, *23*, 4067.
(8) Fujii, Y.; Tamai, Y.; Konishi, T.; Yamakawa, H. *Macromolecules* **1991**, *24*, 1608.
(9) Takaeda, Y.; Yoshizaki, T.; Yamakawa, H. *Macromolecules* **1993**, *26*, 3742.
(10) Yoshizaki, T.; Hayashi, H.; Yamakawa, H. *Macromolecules* **1993**, *26*, 4037.
(11) Dehara, K.; Yoshizaki, T.; Yamakawa, H. *Macromolecules* **1993**, *26*, 5137.
(12) Abe, F.; Horita, K.; Einaga, Y.; Yamakawa, H. *Macromolecules* **1994**, *27*, 725.
(13) Abe, F.; Einaga, Y.; Yoshizaki, T.; Yamakawa, H. *Macromolecules* **1993**, *26*, 1884.
(14) Abe, F.; Einaga, Y.; Yamakawa, H. *Macromolecules* **1993**, *26*, 1891.
(15) Horita, K.; Abe, F.; Einaga, Y.; Yamakawa, H. *Macromolecules* **1993**, *26*, 5067.
(16) Yamakawa, H.; Stockmayer, W. H. *J. Chem. Phys.* **1972**, *57*, 2843.
(17) Yamakawa, H.; Shimada, J. *J. Chem. Phys.* **1985**, *83*, 2607.
(18) Shimada, J.; Yamakawa, H. *J. Chem. Phys.* **1986**, *85*, 591.
(19) Yamakawa, H. *Macromolecules* **1993**, *26*, 5061.
(20) Yamakawa, H.; Abe, F.; Einaga, Y. *Macromolecules*, following paper in this issue.
(21) Rubingh, D. N.; Yu, H. *Macromolecules* **1976**, *9*, 681.
(22) Einaga, Y.; Abe, F.; Yamakawa, H. *J. Phys. Chem.* **1992**, *96*, 3948.
(23) Berry, G. C. *J. Chem. Phys.* **1966**, *44*, 4550.
(24) Bawn, C. E. H.; Freeman, R. F. J.; Kamalidin, A. R. *Trans. Faraday Soc.* **1950**, *46*, 862.
(25) Norisuye, T.; Fujita, H. *ChemTracts: Macromol. Chem.* **1991**, *2*, 293.
(26) Springer, J.; Ueberreiter, K.; Moeller, E. *Z. Elektrochem.* **1965**, *69*, 494.
(27) Cherayil, B. J.; Douglas, J. F.; Freed, K. F. *J. Chem. Phys.* **1985**, *83*, 5293.
(28) For the contribution of the ternary-cluster integral, see also ref 19.
(29) Domb, C.; Barrett, A. J. *Polymer* **1976**, *17*, 179.
(30) Yamakawa, H.; Fujii, M. *J. Chem. Phys.* **1973**, *58*, 1523.